APPLIED PHYSICS LETTERS **104**, 204102 (2014)

An exact field solution of contact resistance and comparison with the transmission line model

Peng Zhang[a] and Y. Y. Lau
Department of Nuclear Engineering and Radiological Sciences, University of Michigan, Ann Arbor, Michigan 48109-2104, USA

(Received 14 January 2014; accepted 8 May 2014; published online 21 May 2014)

Based on the exact solution of the electric field, the contact resistance is calculated and compared with the widely used lumped-circuit transmission line model. Our model fully accounts for the spreading resistance, and is applicable to arbitrary contact size, film thickness, and resistivity in different parts forming the contact. The regimes dominated by the specific contact resistance or by the spreading resistance are identified and compared with experimental data. © *2014 AIP Publishing LLC*. [http://dx.doi.org/10.1063/1.4878841]

Contact resistance is a fundamental limiting factor to modern electronics performance,[1] especially for novel materials with extremely high conductivity used to build conducting channels.[2] How to accurately characterize contact resistance is an important issue.

In 1972, Berger[1] introduced the well-known transmission line model (TLM) to study metal-semiconductor contact.[3] In TLM, the specific contact resistance ρ_c is approximated by lumped circuit elements, and the conducting layer is assumed to be of zero thickness, with sheet resistance ρ_{sh} (Fig. 1). The TLM does not correctly include the spreading resistance caused by current crowding/spreading.[4–6] To include the spreading resistance, Berger added a "virtual" specific contact resistance[1] in his extended TLM (ETLM).

In this Letter, we provide the exact field solution to a model (Fig. 1(a)) and compare the results with TLM and ETLM (Fig. 1(b)). Our model consists of two bulk regions, I, and II, whose dimensions (h_1, h_2, a, b) and electrical resistivity (ρ_1, ρ_2) are specified in Fig. 1(a). An infinitesimally thin interface layer, of specific interfacial resistivity ρ_c (also termed specific contact resistivity), is sandwiched between Regions I and II. Current flows from terminal EF to BC. The terminal EF is at voltage V_0, and BC is grounded. The other boundaries, ED, CD, BO, OA, and FA are electrically insulated. Across the (infinitesimally thin) interface OD, the boundary conditions are: $J_z = -(1/\rho_1)\partial\Phi_I/\partial z = -(1/\rho_2)\partial\Phi_{II}/\partial z$; $\rho_c J_z = \Phi_{II}(y, z = 0^-) - \Phi_I(y, z = 0^+)$, where J_z is the normal component of current density crossing the interface OD, and $\Phi_{\mathrm{I}}(y,z)$ and $\Phi_{\mathrm{II}}(y,z)$ are the potential in Regions I and II, respectively. We should note that the potential distribution in Fig. 1(a) is very difficult to solve accurately by Finite Element Method (FEM) based codes, especially if there is a large contrast among the geometric ratios or resistivity ratios. Here, following Ref. 7, we use Fourier series expansion method to solve for $\Phi_{\mathrm{I}}(y,z)$ and $\Phi_{\mathrm{II}}(y,z)$ exactly, for arbitrary values of h_1, h_2, a, b ($>a$), ρ_1, ρ_2, and ρ_{c}. This paper extends Ref. 7 by including the interface resistance ρ_{c}. Note that ρ_1 and ρ_2 have units in Ω-m whereas ρ_{c} is in Ω-m^2.

In Fig. 1(a), the total resistance, R_T, from EF to BC may be calculated exactly, $R_T = \rho_2(b-a)/(h_2 W) + (\rho_2/2\pi W)\bar{R}_c^{Total}$, where the first term represents the resistance of the thin film from EF to DG, and the second term represents the total contact resistance, $\bar{R}_c^{Total}$ (normalized to $\rho_2/2\pi W$). Here, W denotes the channel width in the dimension perpendicular to the paper. We further decompose $\bar{R}_c^{Total} = \bar{R}_{\text{interface}} + \bar{R}_I + \bar{R}_s$, where $\bar{R}_{\text{interface}} = 2\pi\rho_c/(\rho_2 a)$ represents the resistance in the interface layer, $\bar{R}_I = 2\pi\rho_1 h_1/(\rho_2 a)$ represents the resistance of Region I (from OD to BC), and the remaining term $\bar{R}_s$ represents the spreading resistance (constriction resistance) due to current crowding near the contact region. We find

$$\bar{R}_s = 2\pi\frac{\rho_1}{\rho_2}\sum_{n=1}^{\infty} B_n b_n \frac{\sin(c_n a)}{c_n a} - 2\pi\frac{b-a}{h_2} - 2\pi\frac{\rho_c}{\rho_2 a}, \tag{1}$$

where $b_n = \coth(c_n h_2) + c_n\rho_c/\rho_2$, $c_n = (n - 1/2)\pi/b$, and B_n ($n = 1, 2, 3, \ldots$) is solved from the matrix

$$\frac{\rho_1}{\rho_2}(n - 1/2)B_n + \sum_{m=1}^{\infty} B_m b_m \gamma_{nm} = \frac{2}{\pi}\frac{\sin(c_n a)}{c_n a}, \tag{2}$$

with $\gamma_{nm} = \sum_{k=1}^{\infty} k g_{nk} g_{mk} \coth(k\pi h_1/a)$, $g_{mn} = 2\int_0^1 dx \cos(n\pi x)\cos(c_m a x)$. When $\rho_{\mathrm{c}} = 0$, Eqs. (1) and (2) recover Eqs. (A7) and (A3b) of Ref. 7. In terms of B_n, we record the exact

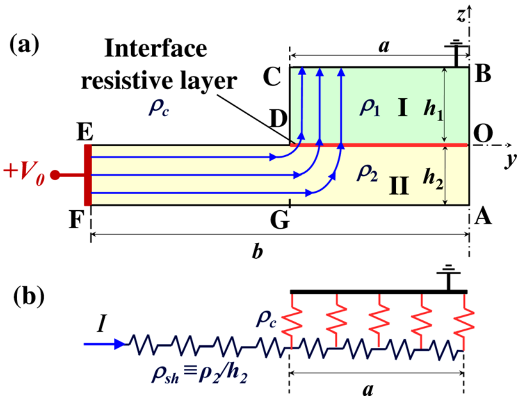

FIG. 1. (a) Electrical contact and (b) its TLM. In (a), an infinitesimally thin resistive interface layer is sandwiched between Regions I and II.

---

[a] Author to whom correspondence should be addressed. Electronic mail: umpeng@umich.edu

0003-6951/2014/104(20)/204102/3/$30.00

expression for the potential in Region II, $\Phi_{II}(y,z) = V_0 + \sum_{n=1}^{\infty} B_n \cos(c_n y)\cosh[c_n(z+h_2)]/\sinh(c_n h_2)$. See Ref. 7 for the detailed derivation of these results and a discussion of their convergence properties. In the numerical calculations below, we fix $a/b = 1/30$.

Figure 2 plots $\bar{R}_{\text{interface}}$, $\bar{R}_s$, and $\bar{R}_c^{Total}$ as a function of a/h_2 for various $r_c = \rho_c/\rho_2 h_2$. To focus on the interface and spreading resistivity, we have set $\rho_1/\rho_2 = 0.01$ and $h_1/h_2 = 0.1$ so that the resistance in Region I, $\bar{R}_I$, is negligible, as shown by the dotted curve in Fig. 2(a). There is always a minimum of $\bar{R}_s$ near $a/h_2 \sim 1$ (Fig. 2(b)), while $\bar{R}_{\text{interface}}$ decreases as a/h_2 increases. When $a/h_2 < 1$, both $\bar{R}_{\text{interface}}$ and $\bar{R}_s$ contribute appreciably to $\bar{R}_c^{Total}$. When $a/h_2 > 1$, the contribution from $\bar{R}_{\text{interface}}$ decreases and is eventually taken over by that of $\bar{R}_s$. From Fig. 2(c), it is clear that for a given aspect ratio a/h_2, $\bar{R}_c^{Total}$ increases with the interface resistivity r_c. For a given r_c, $\bar{R}_c^{Total}$ decreases as a/h_2 increases, converging to a constant value that depends on $\bar{R}_s$. The a/h_2 value beyond which $\bar{R}_c^{Total}$ approaches a constant increases as r_c increases. For comparison, the dashed lines in Fig. 2(c) plot the well-known TLM expression[1,3,4] for the total contact resistance (in the limit $\rho_1 = 0$), $\bar{R}_c^{TLM} = 2\pi\sqrt{r_c}\coth[(a/h_2)/\sqrt{r_c}]$. When $r_c < 1$, TLM ignores the important effects of current crowding. For $r_c > 1$, TLM is a good approximation to $\bar{R}_c^{Total}$. Berger's ETLM[1,4] gives $\bar{R}_c^{ETLM} = 2\pi\sqrt{r_c + 0.19}\coth[(a/h_2)/\sqrt{r_c + 0.19}]$, which is also plotted in Fig. 2(c) as dotted lines. Though semi-empirical, ETLM provides a much more accurate approximation to $\bar{R}_c^{Total}$ than TLM for $r_c < 1$, as shown in Fig. 2(c). However, the error of ETLM is still appreciable for $a/h_2 < 0.2$ with $r_c < 0.2$.

Figure 3 plots $\bar{R}_c^{Total}$ as a function of r_c for various a/h_2. For a given r_c, $\bar{R}_c^{Total}$ decreases as a/h_2 increases. For a given a/h_2, $\bar{R}_c^{Total}$ decreases as r_c decreases, and converges to $\bar{R}_s = 2\pi a/h_2 - 4\ln[\sinh(\pi a/2h_2)]$ as $r_c \to 0$.[8,9] It is important to note that the contact resistance $\bar{R}_c^{Total}$ does not vanish even with ideal contact interface of $r_c = 0$. Once more, TLM can be used to evaluate the contact resistance if $r_c > 2$, ETLM may be used to evaluate the contact resistance when $r_c > 0.2$, and $a/h_2 \geq 0.2$.

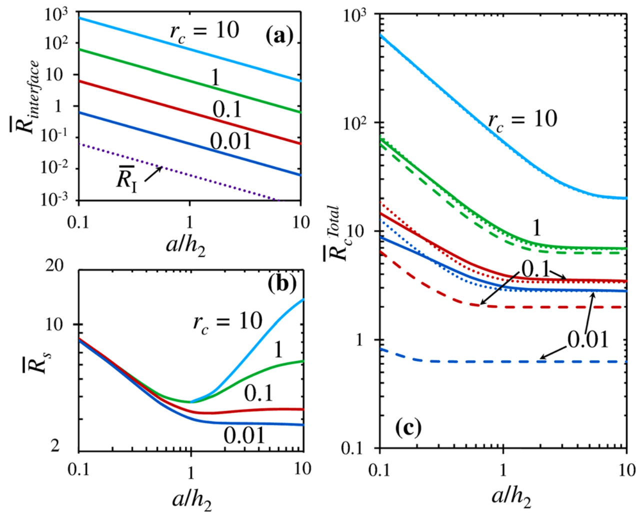

FIG. 2. (a) $\bar{R}_{\text{interface}}$, (b) $\bar{R}_s$, (c) $\bar{R}_c^{Total}$ as function of a/h_2, for various $r_c = \rho_c/\rho_2 h_2$ in Fig. 1(a). The TLM (dashed lines) and the ETLM (dotted lines) are shown in (c) for comparison.

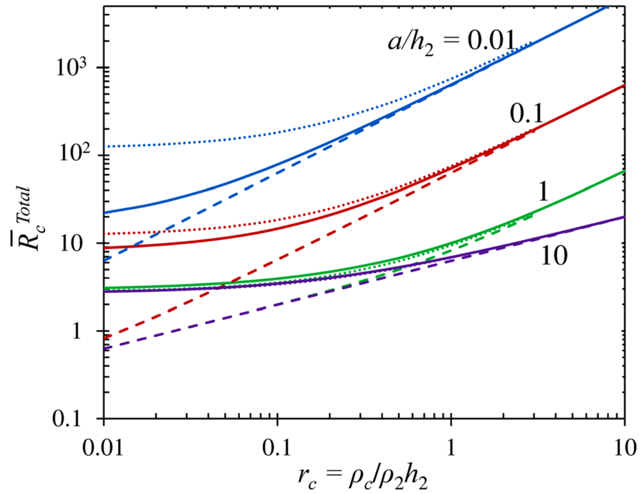

FIG. 3. $\bar{R}_c^{Total}$ as a function of $r_c = \rho_c/\rho_2 h_2$ for various a/h_2 in Fig. 1(a), using the same set of parameters as Fig. 2. The dashed lines are for TLM, and the dotted lines are for ETLM.

Figure 4 shows the effect of R_I, the resistance in region I (Fig. 1(a)), fixing $r_c = 1$. It is important to note that even though the interface resistivity is kept constant, the spreading resistance $\bar{R}_s$ still increases with ρ_1/ρ_2 and h_1/h_2. Thus, the total contact resistance $\bar{R}_c^{Total}$ also increases with ρ_1/ρ_2 and h_1/h_2.

If R_I represents the electrode resistance in Fig. 1(b), it can be eliminated using a highly conductive electrode. It is then important to determine whether the measured contact resistance is dominated by the specific interface resistance $\bar{R}_{\text{interface}}$ or by the spreading resistance $\bar{R}_s$ due to current crowding.[9] Figure 5 shows $\bar{R}_s/\bar{R}_c^{Total}$ for various aspect ratio a/h_2 and resistivity ratio $r_c = \rho_c/\rho_2 h_2$. Again, we set $\rho_1/\rho_2 = 0.01$ and $h_1/h_2 = 0.1$ to minimize the effect of Region I (Fig. 1(a)). Qualitatively, $\bar{R}_s$ is an important

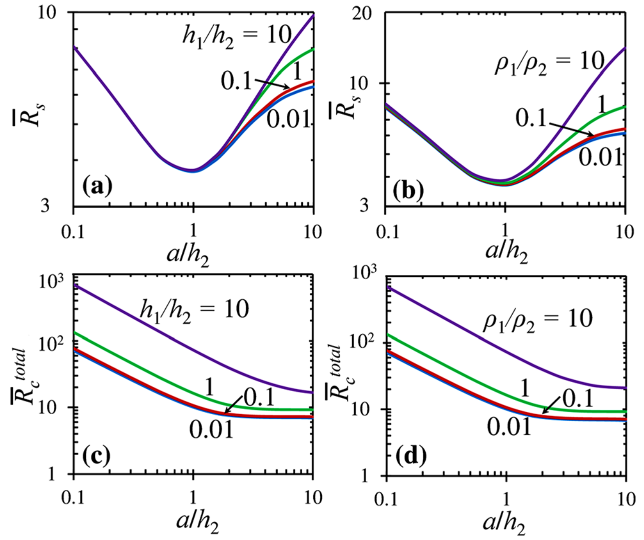

FIG. 4. (a) and (b) $\bar{R}_s$ as a function of a/h_2 for various h_1/h_2 at $\rho_1/\rho_2 = 1$, and for various ρ_1/ρ_2 at $h_1/h_2 = 1$, respectively; (c) and (d) $\bar{R}_c^{Total}$ as a function of a/h_2 for various h_1/h_2 at $\rho_1/\rho_2 = 1$, and for various ρ_1/ρ_2 at $h_1/h_2 = 1$, respectively.

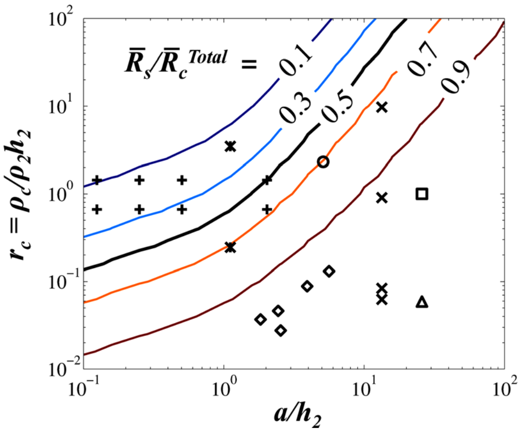

FIG. 5. Contour plot of $\bar{R}_s/\bar{R}_c^{Total}$ as a function of a/h_2 and $r_c = \rho_c/\rho_2 h_2$. Symbols represent previous experiments: ○ for Au/Ge-GaAs,[10] ◇ for Cu-Graphite,[4] + for Al-Si,[1] Δ for Ag-Si/TiOx,[11] □ for Ag-Si,[11] × for Ti/Al/Ni/Cu-AlGaN/GaN,[12] and * for SiC-p^{++}-SiC-n.[13]

(unimportant) contribution to $\bar{R}_c^{Total}$ if $\bar{R}_s/\bar{R}_c^{Total} > 0.5$ ($\bar{R}_s/\bar{R}_c^{Total} < 0.5$). The experimental data of some measured contact resistance[1,4,10–13] are superimposed in Fig. 5. Many cases with dominant spreading resistance ($\bar{R}_s/\bar{R}_c^{Total} > 0.5$) are shown. In this regime, the TLM model is likely to *overestimate* the true specific contact resistivity ρ_c, as seen from Fig. 3; Equation (1) or Figs. 2 and 3 would give a more accurate evaluation.

As a final note, we recall the recent debate on metal-graphene contact, as to whether the current flow path is confined to the edge of the contact, or distributed through the contact area.[14–16] From the above analysis (e.g., Fig. 2(c)), it would seem that the answer depends on the specific interface contact resistivity ρ_c. Qualitatively, if ρ_c is small, i.e., a "good" contact is formed, then the dominant component of the contact resistance is due to spreading resistance; the current flow path is more likely to be confined to the edge of the contact.[9] In contrast, if ρ_c is large, then the dominant component of the contact resistance is due to interface resistivity; the current would distribute more uniformly over the contact area. The current flow patterns in a closely related model are shown in Ref. 7. Some issues in experimental measurement of spreading resistance (or constriction resistance) are addressed in Ref. 17.

This work was supported by AFOSR Grant No. FA9550-09-1-0662 and L-3 Communications Electron Devices Division.

[1] H. H. Berger, Solid State Electron. **15**, 145–158 (1972).
[2] S. Datta, *Quantum Transport: Atom to Transistor* (Cambridge University Press, New York, 2005).
[3] D. K. Schroder, *Semiconductor Material and Device Characterization*, 2 ed. (Wiley & Sons, New York, 1998), p. 149.
[4] E. Woelk, H. Krautle, and H. Beneking, IEEE Trans. Electron Devices **ED-33**(1), 19 (1986).
[5] W. Loh, S. Swirhun, T. Schreyer, R. Swanson, and K. Saraswat, IEEE Trans. Electron Devices **ED-34**(3), 512 (1987).
[6] S. Schuldt, Solid-State Electron. **21**, 715–719 (1978).
[7] P. Zhang, D. Hung, and Y. Y. Lau, J. Phys. D: Appl. Phys. **46**, 065502 (2013); Corrigendum **46**, 209501 (2013).
[8] P. M. Hall, Thin Solid Films **1**(4), 277–295 (1968).
[9] Peng Zhang, Y. Y. Lau, and R. S. Timsit, IEEE Trans. Electron Devices **59**, 1936 (2012).
[10] L. Mak, C. Rogers, and D. Northrop, J. Phys. E: Sci. Instrum. **22**, 317–321(1989).
[11] L. Dobrzański, M. Musztyfaga, A. Drygała, and P. Panek, J. Achiev. Mater. Manuf. Eng. **41**(1–2), 57 (2010).
[12] Y. Wong, Y. Chen, J. Maa, H. Yu, Y. Tu, C. Dee, C. Yap, and E. Chang, Appl. Phys. Lett. **103**, 152104 (2013).
[13] N. Thierry-Jebali, A. Vo-Ha, D. Carole, M. Lazar, G. Ferro, D. Planson, A. Henry, and P. Brosselard, Appl. Phys. Lett. **102**, 212108 (2013).
[14] K. Nagashio, T. Nishimura, K. Kita, and A. Toriumi, Appl. Phys. Lett. **97**, 143514 (2010).
[15] A. Franklin, S. Han, A. Bol, and W. Haensch, IEEE Electron Device Lett. **32**(8), 1035 (2011).
[16] P. Solomon, IEEE Electron Device Lett. **32**(3), 246 (2011).
[17] P. Zhang, Y. Y. Lau, and R. S. Timsit, "Spreading Resistance of Contact Spot on a Thin Film," Proc. of the 59th IEEE Holm Conf. on Electrical Contacts (Newport, RI, 2013).